Einstein-Podolsky-Rosen Entanglement of Narrow-Band Photons from Cold Atoms

Jong-Chan Lee, Kwang-Kyoon Park, Tian-Ming Zhao, and Yoon-Ho Kim*
Department of Physics, Pohang University of Science and Technology (POSTECH), Pohang 37673, Korea
(Received 30 September 2016; published 13 December 2016)

Einstein-Podolsky-Rosen (EPR) entanglement introduced in 1935 deals with two particles that are entangled in their positions and momenta. Here we report the first experimental demonstration of EPR position-momentum entanglement of narrow-band photon pairs generated from cold atoms. By using two-photon quantum ghost imaging and ghost interference, we demonstrate explicitly that the narrow-band photon pairs violate the separability criterion, confirming EPR entanglement. We further demonstrate continuous variable EPR steering for positions and momenta of the two photons. Our new source of EPR-entangled narrow-band photons is expected to play an essential role in spatially multiplexed quantum information processing, such as, storage of quantum correlated images, quantum interface involving hyperentangled photons, etc.

DOI: 10.1103/PhysRevLett.117.250501

Entanglement, initially explored experimentally with the polarization states of a pair of photons [1,2], has now been demonstrated in a variety of physical systems, e.g., two spontaneous parametric down-conversion (SPDC) photons [3,4], two-mode squeezed states of optical fields [5,6], trapped ions [7,8], neutral atoms [9,10], and artificial quantum systems [11,12]. The gedanken experiment proposed by Einstein-Podolsky-Rosen (EPR) in 1935, on the other hand, involves a pair of particles that are entangled in their positions and momenta [13–15]. In addition to fundamental interests, EPR entanglement is essential in quantum imaging and quantum metrology [16–19]. Here we report EPR position-momentum entanglement of narrow-band (∼MHz) photon pairs generated from $\chi^{(3)}$ spontaneous four-wave mixing (SFWM) in a cold atomic ensemble. By using two-photon quantum ghost imaging and interference [20,21], we demonstrate explicitly that the narrow-band photon pairs violate the separability criterion, confirming EPR position-momentum entanglement. We further demonstrate continuous variable EPR steering for positions and momenta of the two photons [22–28]. To the best of our knowledge, this is the first experimental demonstration of EPR entanglement and EPR steering of position-momentum degrees of freedom of narrow-band photon pairs, well suited for spatially multiplexed quantum information processing, storage of quantum images, quantum interface involving hyperentangled photons, etc. [29–34].

The position-momentumlike continuous variable feature of EPR entanglement has been explored initially by using quadrature-phase amplitudes of two-mode squeezed states [5,6]. Genuine EPR position-momentum entanglement of photon pairs became available later by the SPDC process in a bulk crystal [14,15] and is thought to be essential in quantum imaging and quantum metrology [16–19]. The EPR-entangled SPDC photons, however, are inherently broadband, typically on the order of several THz in bandwidth. This large bandwidth makes the source unsuitable for interfacing with quantum memory based on atom-photon coherent interaction, which typically has the working bandwidth of a few MHz [30–34]. Although narrowband entangled photon pairs can be generated via cavity-enhanced SPDC [35,36], the optical cavity necessary for bandwidth narrowing eradicates EPR position-momentum entanglement between the photon pairs. Spontaneous four-wave mixing (SFWM) in a cold atom medium can generate narrow-band entangled photons without the need for optical cavities [37–39], but, to date, no EPR position-momentum entanglement has been reported via SFWM. In this work, we demonstrate EPR position-momentum entanglement of a photon pair generated via cold atom-based SFWM by using quantum ghost interference and ghost imaging. It is shown that the photon pair violates the position-momentum continuous variable separability criterion and satisfies the EPR steering condition [22–25].

The experimental schematic is shown in Fig. 1. The SFWM photon pairs are generated from an ensemble of cold 87 Rb atoms in a cigar-shaped 2D magneto-optical trap (MOT) [38–40]. When the counterpropagating pump (ω_p) and coupling (ω_c) lasers are applied to the cold atom cloud, the Stokes (ω_s) and anti-Stokes (ω_{as}) photons are generated via SFWM. The atomic four-level double-Λ system used for SFWM consists of $|1\rangle \equiv |5S_{1/2}(F=1)\rangle$, $|2\rangle \equiv |5S_{1/2}(F=2)\rangle$, $|3\rangle \equiv |5P_{1/2}(F=2)\rangle$, and $|4\rangle \equiv |5P_{3/2}(F=2)\rangle$. All the atoms are initially prepared in the ground state $|1\rangle$ [38]. The pump laser is red detuned by $\Delta = 2\pi \times 78.5$ MHz from the $|1\rangle \leftrightarrow |4\rangle$ transition and the coupling laser is resonant to the $|2\rangle \leftrightarrow |3\rangle$ transition. The SFWM photon pair is collected at the angle of 2.5° with respect to the pump or coupling laser directions and the polarization states of the Stokes and anti-Stokes photons are chosen by wave plates (WP) and polarization beam splitters (PBS). The angle is exaggerated in Fig. 1 for clarity. The SFWM photon pairs are measured with single-photon detectors (SPD, Perkin Elmer SPCM-AQRH-13FC) and

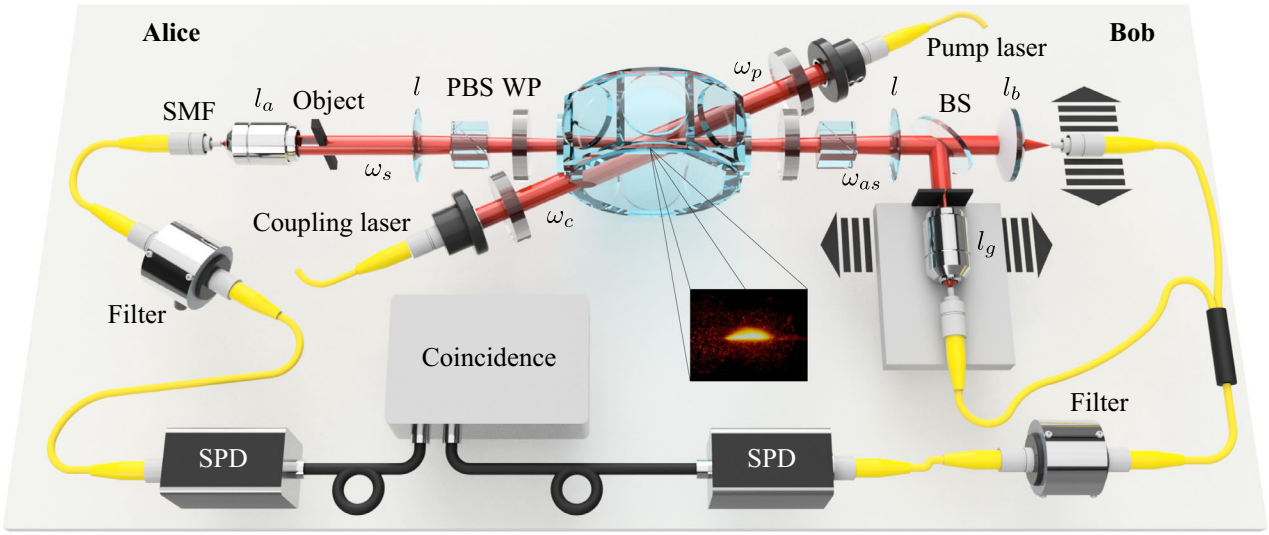

FIG. 1. Schematic of the experiment. The Stokes (ω_s) and anti-Stokes (ω_{as}) photon pair with EPR position-momentum entanglement is generated in the 87 Rb cold atom cloud by applying the pump (ω_p) and coupling (ω_c) lasers. Wave plates (WP) and polarizing beam splitters (PBS) are used to set the proper polarization states. To optically relay the diverging Stokes and anti-Stokes photons to Alice and Bob, the lenses l are used ($f = 400$ mm). The SFWM photon pairs are measured with single-photon detectors (SPD). SMF and BS refer to the single-mode fiber and the beam splitter, respectively.

coincidence events are recorded with time-tagging electronics (SensL HRM-TDC). It is important to note that, to generate a photon pair with EPR position-momentum entanglement, the pump and coupling lasers should not be tightly focused.

The optical depth (OD) of our cigar-shaped MOT was measured to be about 50. The experiment is repeated every 10 ms: 9 ms is used for preparation of the cold atomic ensemble, and 1 ms is dedicated to SFWM for generating narrow-band photon pairs. Two different values of pump power are used for two different pumping conditions. When the pump field is nearly collimated with diameter $2w_0 = 2.16$ mm, the pump power was set at 1.5 mW. When the pump is focused to $2w_0 = 235$ μm with a lens of focal length 500 mm, the pump power was 60 μW. The Rayleigh length in this case was $2z_R = 11$ cm, which sufficiently covers the atomic ensemble longitudinally. The coupling field is 3 mW in power and 3 mm in diameter. The polarization states of pump, Stokes, coupling, and anti-Stokes fields are chosen to be ↻, ↺, ↺, ↻, where ↻ and ↺ represents right-circular and left-circular polarizations as seen from the receiver, respectively. To block the pump and coupling lasers, temperature controlled solid etalon filters (470 MHz full-width-at-half-maximum transmission bandwidth; 21 GHz free spectral range) are placed before the detectors.

The two-photon quantum state generated from SFWM can be written as [38,39]

$$|\Psi\rangle \propto \int d\omega_{as} d\omega_s d\vec{\kappa}_s d\vec{\kappa}_{as} \chi^{(3)}(\omega_{as}, \omega_s) \mathrm{sinc}(\Delta k L/2) \times \mathcal{C}_\perp(\vec{\kappa}_+, \vec{\kappa}_-) \hat{a}^\dagger_{\vec{\kappa}_s} \hat{a}^\dagger_{\vec{\kappa}_{as}} |0\rangle, \quad (1)$$

where ω_{as} and ω_s are the frequencies of anti-Stokes and Stokes photons, $\chi^{(3)}(\omega_{as}, \omega_s)$ is the third-order nonlinear susceptibility of the medium, $\Delta k = (\vec{k}_p + \vec{k}_c - \vec{k}_s - \vec{k}_{as}) \cdot \vec{z}$ is the longitudinal phase mismatch along the direction $\vec{z}$ of the 2D MOT of length L, and $\hat{a}^\dagger_{\vec{\kappa}_s}$ ($\hat{a}^\dagger_{\vec{\kappa}_{as}}$) is the creation operator of photons with the transverse wave vector $\vec{\kappa}_s$ ($\vec{\kappa}_{as}$). Here $\vec{k}_p$, $\vec{k}_c$, $\vec{k}_s$, $\vec{k}_{as}$ are the wave vectors of pump, coupling, Stokes, and anti-Stokes photons within the medium, respectively. The transverse components of the wave vectors are $\vec{\kappa}_s$ and $\vec{\kappa}_{as}$ for the Stokes and the anti-Stokes photons, respectively. The transverse correlation function is $\mathcal{C}_\perp(\vec{\kappa}_+, \vec{\kappa}_-) = \tilde{\mathcal{E}}_+(|\vec{\kappa}_+|)\tilde{\mathcal{E}}_-(|\vec{\kappa}_-|/2)$, where $\vec{\kappa}_\pm = \vec{\kappa}_{as} \pm \vec{\kappa}_s$ and $\tilde{\mathcal{E}}_\pm$ are envelopes with standard deviations $\sigma_\pm$. For a perfectly EPR-entangled photon pair, $\tilde{\mathcal{E}}_+(|\vec{\kappa}_+|) \to \delta(\vec{\kappa}_+)$ and $\tilde{\mathcal{E}}_-(|\vec{\kappa}_-|) \to 1$ such that the transverse correlation function becomes $\mathcal{C}_\perp(\vec{\kappa}_+, \vec{\kappa}_-) \to \delta(\vec{\kappa}_+)$. Here, it is assumed that the coupling field is a plane wave with wave vector $\vec{k}_c$ and the medium is larger than the spatial envelope of the pump. Full calculation details are given in the Supplemental Material [41].

To confirm EPR entanglement and EPR steering for the position-momentum variables, we make use of the quantum ghost imaging and interference effects [20,21]. Roughly speaking, in ghost interference and ghost imaging experiments with a pair of photons, an object is placed in the path of one photon which is then detected by a detector with no spatial resolution and the other photon is measured with a scanning detector with spatial resolution. The single count rate of the scanning detector does not reveal any image or interference, but, strangely (hence the term "ghost"), ghost

image or ghost interference due to the object appears in the coincidence count rate between the two detectors [20,21].

On Alice's side, we place the object, a metal block of width = 1.23 mm, in front of the objective lens l_a with focus $f_a = 13.5$ mm and numerical aperture (NA) = 0.25. A single-mode fiber (SMF) is placed at the focus of the objective lens l_a for photon detection. The effective shape of the object, considering the transverse dimensions of the object, the SFWM beam (the Stokes photon), the numerical apertures of the objective lens, and the SMF, is a double slit. We thus expect to observe ghost interference and ghost imaging corresponding to the effective double slit placed at the location of the object. The scanning detector is placed on Bob's side. The two-photon ghost interference and ghost imaging measurements require different optical setups for measurement. The transmission or reflection at the beam splitter (BS) selects whether to observe the ghost interference or the ghost imaging, respectively [14,15]. For the ghost interference measurement, the SMF tip is scanned at the focus of the lens l_b with focus $f_b = 25.4$ mm. For the ghost imaging measurement, the measurement setup includes a narrow vertical slit of 0.4 mm in width, which defines the imaging resolution, the objective lens l_g ($f_g = 13.5$ mm, NA = 0.25), and an SMF. The whole setup is mounted on a translation stage and scanned.

It is well known that a pair of classically correlated photons in their positions and in their momenta can lead to ghost imaging and ghost interference, respectively [46–50]. It is, however, fundamentally impossible to observe both ghost imaging and ghost interference with a classical position-correlated or momentum-correlated photon pairs [46,47]. On the other hand, if a photon pair is EPR entangled, i.e., quantum correlation exits simultaneously in positions and momenta of the photons, both ghost imaging and ghost interference may be observed by choosing the appropriate measurement basis [14,15]. Thus, experimental observation of both high visibility quantum ghost interference as well as high contrast quantum ghost imaging from the experimental setup in Fig. 1 can be used to confirm EPR position-momentum entanglement of the photon pair.

The experimental data for quantum ghost interference and ghost imaging are shown in Fig. 2. The coincidence count is normalized to the product of the single counts at the two detectors to remove the effects of single count variations to the coincidence count. When the pump laser is collimated (beam diameter $2w_0 = 2.16$ mm), the data clearly exhibit high contrast ghost interference, Fig. 2(a), and ghost imaging, Fig. 2(b), indicating a high degree of EPR position-momentum entanglement. When the pump laser is focused ($2w_0 = 235$ μm), the quality of the ghost interference, Fig. 2(c), and ghost image, Fig. 2(d), are reduced, signaling reduced EPR entanglement.

Theoretically, ghost interference can be calculated, for a given object transfer function, as follows. The effective

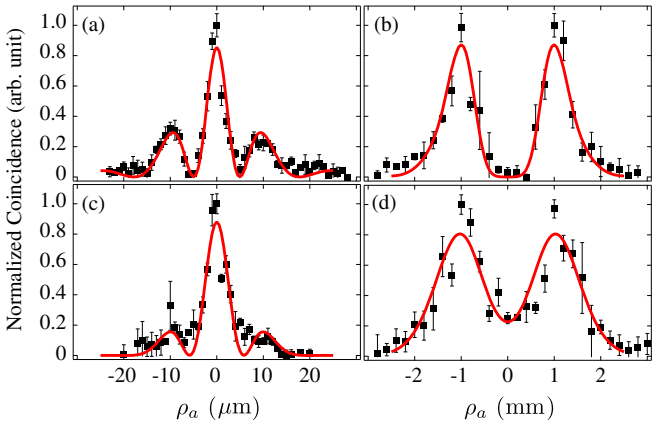

FIG. 2. Experimental results. When the pump laser is collimated (beam diameter $2w_0 = 2.16$ mm), quantum ghost interference (a) and ghost image (b) of the object are clearly observed. From these data, we obtain clear signatures of EPR entanglement and EPR steering for the position-momentum variables. See text for details. When the pump laser is focused ($2w_0 = 235$ μm), the quality of the ghost interference (c) and ghost image (d) are reduced, signaling reduced EPR entanglement. Each point of the experimental data was accumulated for 60 s. The solid red lines are numerical fits of the experimental data. Error bars represent statistical error of ± 1 standard deviation.

double slit located at the object plane on Alice's side causes quantum ghost interference to occur when Bob scans his detector at the far zone, i.e., at the focus of the lens l_b. Assuming that in Alice's measurement plane, her SMF is located at the optical axis defined by the source and the lenses l, l_a, and l_b ($\vec{\rho}_a = 0$), the normalized coincidence count rate $G^{(2)}(\vec{\rho}_b)$ is given by

$$\left| \int d\vec{\kappa}_s d\vec{\kappa}_{as} \mathcal{C}_\perp(\vec{\kappa}_+, \vec{\kappa}_-) \mathcal{T}\left(\frac{\lambda_s f}{2\pi}\vec{\kappa}_s\right) \exp\left(-i\frac{f}{f_b}\vec{\kappa}_{as}\cdot\vec{\rho}_b\right)\right|^2,$$

where λ_s is the wavelength of the Stokes photons, f is the focal length of the lens l, $\mathcal{T}(\vec{\rho}_o)$ is the object transfer function defined by the effective double slit at the object plane $\vec{\rho}_o$. As described earlier, when the position-momentum correlation is ideal so that $\mathcal{C}_\perp(\vec{\kappa}_+, \vec{\kappa}_-) = \delta(\vec{\kappa}_+)$, the two-photon correlation function can be described simply as the square of the Fourier transform of the object transfer function: $G^{(2)}(\vec{\rho}_b) \propto |\tilde{\mathcal{T}}[(f/f_b)\vec{\rho}_b]|^2$. When the pump has a finite spatial envelope, i.e., $\mathcal{C}_\perp(\vec{\kappa}_+, \vec{\kappa}_-)$ is not equal to the delta function, the two-photon correlation function degrades from the ideal Fourier transform. The shape of the nonideal ghost interference depends on the two parameters σ_+ and σ_-. By fitting the experimental data to the theoretical calculation, it is possible to obtain σ_+ and σ_-. Using the quantum state in Eq. (1), the uncertainty of the total momentum, Δp_+, is calculated to be $\Delta p_+ = \hbar\sigma_+/\sqrt{2}$. Similarly, the uncertainty of the relative position, Δx_-, is calculated to be $\Delta x_- = \sigma_-^{-1}/\sqrt{2}$.

In the case of ghost imaging, Bob's detection plane is defined by a narrow vertical slit and ghost imaging is obtained by horizontally scanning the whole measurement setup mounted on a translation stage. Assuming that the opening of Bob's narrow slit is located at $\vec{\rho}_b$ and that Alice's SMF is located at $\vec{\rho}_a = 0$, the two-photon correlation function for the ghost imaging setup can be written as

$$G^{(2)}(\vec{\rho}_b) \propto \left| \int d\vec{\kappa}_s d\vec{\kappa}_{as} \mathcal{C}_\perp(\vec{\kappa}_+, \vec{\kappa}_-) \mathcal{T}\left(\frac{\lambda_s f}{2\pi}\vec{\kappa}_s\right) \times \delta\left(\vec{\kappa}_{as} - \frac{\omega}{cf}\vec{\rho}_b\right)\right|^2.$$

Again, when the pump field is a plane wave so that the position-momentum correlation is perfect, i.e., $\mathcal{C}_\perp(\vec{\kappa}_+, \vec{\kappa}_-) = \delta(\vec{\kappa}_+)$, the two-photon correlation function is reduced to $G^{(2)}(\vec{\rho}_b) \propto |\mathcal{T}(-\vec{\rho}_b)|^2$, which is proportional to the square of the object transfer function itself, $|\mathcal{T}(\vec{\rho}_o)|^2$. When the momentum of the pump cannot be described by the delta function, the two-photon correlation function has to be calculated from Eq. (1), which can give a somewhat blurred image of the object. Again, by fitting the experimental data to the theory, we can obtain σ_+ and σ_-. Full calculation details are given in the Supplemental Material [41].

To firmly establish that the SFWM photon pair from the cold atom cloud is EPR position-momentum entangled, it is necessary to check if the photon pair violates a separability criterion using the experimental ghost imaging and ghost interference data in Fig. 2. For the transverse positions (x_1, x_2) and transverse momenta (p_1, p_2) of the two particles, if the two particles are in a separable state, they satisfy the inequality [22–25],

$$\langle(\Delta x_-)^2\rangle\langle(\Delta p_+)^2\rangle \geq |\langle[x_1, p_1]\rangle|^2, \quad (2)$$

where $x_- = x_1 - x_2$ and $p_+ = p_1 + p_2$. Experimental violation of the above inequality directly implies that the two photons are in an entangled state. Another notable criterion which we are interested in is the EPR steering inequality [22–25]. EPR steering is a stricter form of quantum correlation than entanglement such that entanglement is a necessary but not a sufficient condition for EPR steering. Operationally, EPR steering is equivalent to the task of entanglement distribution when one of the two involved parties is untrusted. Therefore, EPR steering allows for, for example, quantum key distribution when one of the parties cannot trust his or her device. The EPR steering is possible, or EPR paradox arises, if the following inequality is satisfied [22–25]:

$$\langle(\Delta x_-)^2\rangle\langle(\Delta p_+)^2\rangle < \frac{1}{4}|\langle[x_1, p_1]\rangle|^2. \quad (3)$$

Our experimental results show a strong violation of the inequality in Eq. (2), hence confirming that the photon pair is EPR position-momentum entangled and satisfies the EPR steering inequality in Eq. (3). By fitting the experimental data in Fig. 2 with the theoretical two-photon correlation functions for ghost interference and ghost imaging, we obtain the joint uncertainties Δx_- and Δp_+. (Full calculation details are given in the Supplemental Material [41].) From Fig. 2(a), we obtain $\Delta p_+ = 1.053 \pm 0.635\hbar$ mm^{-1} and $\Delta x_- = 0.0137 \pm 0.0001$ mm. We thus have $(\Delta x_-)^2(\Delta p_+)^2 = 0.000\,208 \pm 0.000\,177\hbar^2 \ll \hbar^2$. Similarly, from Fig. 2(b), we have $(\Delta x_-)^2(\Delta p_+)^2 = 0.000\,372 \pm 0.000\,055\hbar^2 \ll \hbar^2$. Both results show a strong violation of the separability criterion in Eq. (2) as well as satisfying the EPR steering inequality in Eq. (3).

To study the effect of the spatial profile of the pump to the quality of EPR entanglement of the SFWM photons, we then slightly focused the pump laser so that the beam diameter $2w_0 = 235$ μm at the MOT. The resulting ghost interference and imaging data are shown in Figs. 2(c) and 2(d), respectively. From Fig. 2(c), we obtain $(\Delta x_-)^2(\Delta p_+)^2 = 0.0315 \pm 0.0083\hbar^2 \ngeq \hbar^2$ and from Fig. 2(d), we obtain $(\Delta x_-)^2(\Delta p_+)^2 = 0.00326 \pm 0.00124\hbar^2 \ngeq \hbar^2$. While both results do violate the separability criterion in Eq. (2) and satisfy the EPR steering inequality in Eq. (3), it is clear that the violation of separability, in this case, is weaker than the previous one in which the pump was collimated.

Our narrowband EPR-entangled (i.e., position-momentum entangled) photon pairs have unique advantages over the spontaneous parametric down-conversion (SPDC)-based EPR-entangled photon pairs. Photon pairs from SPDC typically have the bandwidth of a few THz. Although SPDC has been a workhorse in quantum information experiments by demonstrating a variety of entanglement, it is simply not compatible with the atomic quantum memory due to the large bandwidth. While cavity SPDC can exhibit the bandwidth compatible with atomic quantum memory (~MHz), only a certain type of entanglement, e.g., polarization or energy time, is possible with cavity SPDC. Moreover, frequency filtering of SPDC photons via optical cavities cannot lead to position-momentum entanglement of narrowband photons. On the other hand, the EPR-entangled photon pairs generated from a cold atomic ensemble intrinsically have narrow bandwidths on the order of a few MHz which is compatible with atomic quantum memory.

In summary, we demonstrated, for the first time, EPR position-momentum entanglement of narrow-band photon pairs generated from $\chi^{(3)}$ nonlinearity in a cold atomic ensemble via SFWM. We observed both two-photon ghost interference and ghost imaging effects by using the EPR pair-photon source. From the ghost interference and ghost imaging results, we showed explicitly that the photon pair violates the inseparability criterion as well as satisfying the EPR steering inequality, confirming high-quality EPR position-momentum entanglement between the two narrowband photons. We have also explored the effect of pump spatial profile to the degree of EPR entanglement between

the photon pairs. The reported EPR photon pair source is inherently well suited for efficient interaction and storage in quantum memory or repeater and is expected to play an essential role in spatially multiplexed quantum information processing, including quantum imaging and quantum metrology.

This work was supported by Samsung Science & Technology Foundation under Project No. SSTF-BA1402-07.

*yoonho72@gmail.com

[1] S. J. Freedman and J. F. Clauser, Phys. Rev. Lett. **28**, 938 (1972).
[2] A. Aspect, P. Grangier, and G. Roger, Phys. Rev. Lett. **47**, 460 (1981).
[3] Y. H. Shih and C. O. Alley, Phys. Rev. Lett. **61**, 2921 (1988).
[4] C. K. Hong, Z. Y. Ou, and L. Mandel, Phys. Rev. Lett. **59**, 2044 (1987).
[5] Z. Y. Ou, S. F. Pereira, H. J. Kimble, and K. C. Peng, Phys. Rev. Lett. **68**, 3663 (1992).
[6] T. C. Ralph and P. K. Lam, Phys. Rev. Lett. **81**, 5668 (1998).
[7] Q. A. Turchette, C. S. Wood, B. E. King, C. J. Myatt, D. Leibfried, W. M. Itano, C. Monroe, and D. J. Wineland, Phys. Rev. Lett. **81**, 3631 (1998).
[8] M. Riebe *et al.*, Nature (London) **429**, 734 (2004).
[9] E. Hagley, X. Maître, G. Nogues, C. Wunderlich, M. Brune, J. M. Raimond, and S. Haroche, Phys. Rev. Lett. **79**, 1 (1997).
[10] C. W. Chou, H. de Riedmatten, D. Felinto, S. V. Polyakov, S. J. van Enk, and H. J. Kimble, Nature (London) **438**, 828 (2005).
[11] H. Bernien, L. Childress, L. Robledo, M. Markham, D. Twitchen, and R. Hanson, Phys. Rev. Lett. **108**, 043604 (2012).
[12] D. Riste, M. Dukalski, C. A. Watson, G. de Lange, M. J. Tiggelman, Y. M. Blanter, K. W. Lehnert, R. N. Schouten, and L. DiCarlo, Nature (London) **502**, 350 (2013).
[13] A. Einstein, B. Podolsky, and N. Rosen, Phys. Rev. **47**, 777 (1935).
[14] J. C. Howell, R. S. Bennink, S. J. Bentley, and R. W. Boyd, Phys. Rev. Lett. **92**, 210403 (2004).
[15] M. D'Angelo, Y.-H. Kim, S. P. Kulik, and Y. Shih, Phys. Rev. Lett. **92**, 233601 (2004).
[16] K. Wagner, J. Janousek, V. Delaubert, H. Zou, C. Harb, N. Treps, J. F. Morizur, P. K. Lam, and H. A. Bachor, Science **321**, 541 (2008).
[17] G. Brida, M. Genovese, and I. Ruo Berchera, Nat. Photonics **4**, 227 (2010).
[18] C. A. Pérez-Delgado, M. E. Pearce, and P. Kok, Phys. Rev. Lett. **109**, 123601 (2012).
[19] T. Ono, R. Okamoto, and S. Takeuchi, Nat. Commun. **4**, 2426 (2013).
[20] T. B. Pittman, Y. H. Shih, D. V. Strekalov, and A. V. Sergienko, Phys. Rev. A **52**, R3429 (1995).
[21] D. V. Strekalov, A. V. Sergienko, D. N. Klyshko, and Y. H. Shih, Phys. Rev. Lett. **74**, 3600 (1995).
[22] M. D. Reid and P. D. Drummond, Phys. Rev. Lett. **60**, 2731 (1988).
[23] M. D. Reid, Phys. Rev. A **40**, 913 (1989).
[24] S. Mancini, V. Giovannetti, D. Vitali, and P. Tombesi, Phys. Rev. Lett. **88**, 120401 (2002).
[25] L. M. Duan, G. Giedke, J. I. Cirac, and P. Zoller, Phys. Rev. Lett. **84**, 2722 (2000).
[26] P.-A. Moreau, F. Devaux, and E. Lantz, Phys. Rev. Lett. **113**, 160401 (2014).
[27] H. M. Wiseman, S. J. Jones, and A. C. Doherty, Phys. Rev. Lett. **98**, 140402 (2007).
[28] E. G. Cavalcanti, S. J. Jones, H. M. Wiseman, and M. D. Reid, Phys. Rev. A **80**, 032112 (2009).
[29] M. N. O'Sullivan-Hale, I. A. Khan, R. W. Boyd, and J. C. Howell, Phys. Rev. Lett. **94**, 220501 (2005).
[30] P. K. Vudyasetu, R. M. Camacho, and J. C. Howell, Phys. Rev. Lett. **100**, 123903 (2008).
[31] V. Boyer, A. M. Marino, R. C. Pooser, and P. D. Lett, Science **321**, 544 (2008).
[32] Y.-W. Cho, J.-E. Oh, and Y.-H. Kim, Opt. Express **20**, 5809 (2012).
[33] A. Nicolas, L. Veissier, L. Giner, E. Giacobino, D. Maxein, and J. Laurat, Nat. Photonics **8**, 234 (2014).
[34] A. I. Lvovsky and M. G. Raymer, Rev. Mod. Phys. **81**, 299 (2009).
[35] Z. Y. Ou and Y. J. Lu, Phys. Rev. Lett. **83**, 2556 (1999).
[36] X.-H. Bao, Y. Qian, J. Yang, H. Zhang, Z.-B. Chen, T. Yang, and J.-W. Pan, Phys. Rev. Lett. **101**, 190501 (2008).
[37] V. Balić, D. A. Braje, P. Kolchin, G. Y. Yin, and S. E. Harris, Phys. Rev. Lett. **94**, 183601 (2005).
[38] S. Du, J. Wen, and M. H. Rubin, J. Opt. Soc. Am. B **25**, C98 (2008).
[39] Y.-W. Cho, K.-K. Park, J.-C. Lee, and Y.-H. Kim, Phys. Rev. Lett. **113**, 063602 (2014).
[40] Y.-W. Cho, K.-K. Park, J.-C. Lee, and Y.-H. Kim, J. Korean Phys. Soc. **63**, 943 (2013).
[41] See Supplemental Material http://link.aps.org/supplemental/10.1103/PhysRevLett.117.250501, which includes Refs. [42–45], for the detailed theoretical calculations for the two-photon correlation functions for the quantum ghost interference and ghost imaging.
[42] D. S. Tasca, R. M. Gomes, F. Toscano, P. H. Souto Ribeiro, and S. P. Walborn, Phys. Rev. A **83**, 052325 (2011).
[43] J.-C. Lee, Y.-S. Kim, Y.-S. Ra, H.-T. Lim, and Y.-H. Kim, Phys. Rev. A **86**, 042112 (2012).
[44] R. J. Glauber, Phys. Rev. **130**, 2529 (1963).
[45] M. H. Rubin, Phys. Rev. A **54**, 5349 (1996).
[46] R. S. Bennink, S. J. Bentley, R. W. Boyd, and J. C. Howell, Phys. Rev. Lett. **92**, 033601 (2004).
[47] M. D'Angelo, A. Valencia, M. H. Rubin, and Y. Shih, Phys. Rev. A **72**, 013810 (2005).
[48] R. S. Bennink, S. J. Bentley, and R. W. Boyd, Phys. Rev. Lett. **89**, 113601 (2002).
[49] A. Gatti, E. Brambilla, M. Bache, and L. A. Lugiato, Phys. Rev. Lett. **93**, 093602 (2004).
[50] A. I. Lvovsky, B. C. Sanders, and W. Tittel, Nat. Photonics **3**, 706 (2009).